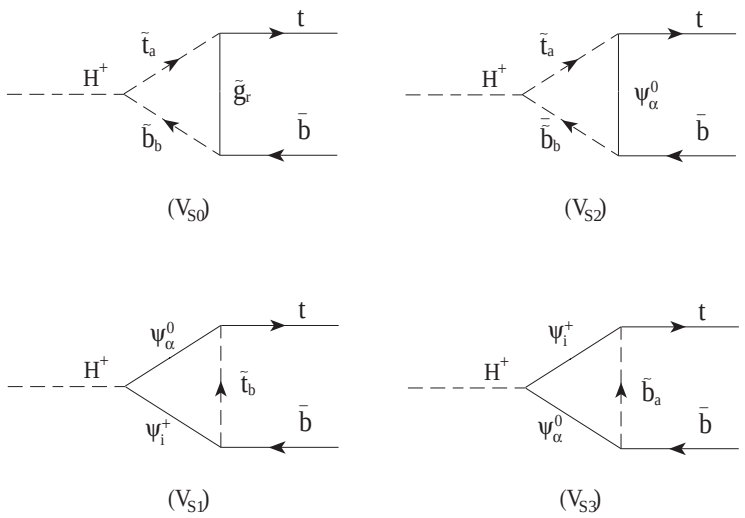

Figure 4.12: *Feynman diagrams, up to one-loop order, for the QCD and electroweak SUSY vertex corrections to the decay process $H^+ \to t\bar{b}$. Each one-loop diagram is summed over all possible values of the mass-eigenstate gluinos ($\tilde{g}_r\,; r = 1, \ldots, 8$), charginos ($\Psi_i^{\pm}\,; i = 1, 2$), neutralinos ($\Psi_\alpha^0\,; \alpha = 1, ..., 4$), stop and sbottom squarks ($\tilde{b}_a, \tilde{t}_b\,; a, b = 1, 2$).*

4.4.1 SUSY vertex diagrams

In this section we will make intensive use of the definitions and formulae of Sec. 2.2.1. We refer the reader there for questions about notation and conventions. Following the labelling of Feynman graphs in Fig. 4.12 we write down the terms coming from virtual SUSY particles.

- Diagram (V_{S0}): Making use of the convention that lower indices are summed over, whereas upper indices (some of them within parenthesis) are just for notational convenience one finds:

$$\begin{aligned} H_L &= 8\pi\alpha_s\, iC_F \frac{G^*_{ab}}{m_t \cot\beta} \quad [R^{(t)}_{1b} R^{(b)*}_{1a} (C_{11} - C_{12}) m_t + R^{(t)}_{2b} R^{(b)*}_{2a} C_{12} m_b \\ &\qquad\qquad + R^{(t)}_{2b} R^{(b*)}_{1a} C_0 m_{\tilde{g}}]\,, \\ H_R &= 8\pi\alpha_s\, iC_F \frac{G^*_{ab}}{m_b \tan\beta} \quad [R^{(t)}_{2b} R^{(b)*}_{2a} (C_{11} - C_{12}) m_t + R^{(t)}_{1b} R^{(b)*}_{1a} C_{12} m_b \\ &\qquad\qquad + R^{(t)}_{1b} R^{(b)*}_{2a} C_0 m_{\tilde{g}}]\,, \end{aligned} \tag{4.54}$$

where the notation for the various 3-point functions is summarized in Appendix A, so that, in eq. (4.54) the C-functions must be evaluated with arguments:

$$C_* = C_*\left(p, p', m_{\tilde{g}}, m_{\tilde{t}_b}, m_{\tilde{b}_a}\right) .$$

and $C_F = (N_C^2 - 1)/2N_C = 4/3$ is a colour factor obtained after summation over colour indices

- Diagram (V_{S1}): Making use of the coupling matrices of eqs. (2.31) and (2.40) we introduce the shorthands

$$A_\pm \equiv A^{(t)}_{\pm ai} \quad \text{and} \quad A^{(0)}_\pm \equiv A^{(t)}_{\pm a\alpha} ,$$

and define the combinations (omitting indices also for $Q^L_{\alpha i}, Q^R_{\alpha i}$)

$$\begin{aligned}
A^{(1)} &= \cos\beta A^*_+ Q^L A^{(0)}_- , & E^{(1)} &= \cos\beta A^*_- Q^L A^{(0)}_- , \\
B^{(1)} &= \cos\beta A^*_+ Q^L A^{(0)}_+ , & F^{(1)} &= \cos\beta A^*_- Q^L A^{(0)}_+ , \\
C^{(1)} &= \sin\beta A^*_+ Q^R A^{(0)}_- , & G^{(1)} &= \sin\beta A^*_- Q^R A^{(0)}_- , \\
D^{(1)} &= \sin\beta A^*_+ Q^R A^{(0)}_+ , & H^{(1)} &= \sin\beta A^*_- Q^R A^{(0)}_+ .
\end{aligned} \tag{4.55}$$

The contribution from diagram (V_{S1}) to the form factors H_R and H_L is then

$$\begin{aligned}
H_R \;= M_L \;& \Big[H^{(1)} \tilde{C}_0 + \\
& + m_b \left(m_t A^{(1)} + M^0_\alpha B^{(1)} + m_b H^{(1)} + M_i D^{(1)} \right) C_{12} \\
& + m_t \left(m_t H^{(1)} + M^0_\alpha G^{(1)} + m_b A^{(1)} + M_i E^{(1)} \right) (C_{11} - C_{12}) \\
& + \left(m_t m_b A^{(1)} + m_t M_i E^{(1)} + M^0_\alpha m_b B^{(1)} + M_i M^0_\alpha F^{(1)} \right) C_0 \Big] , \\
H_L \;= M_R \;& \Big[A^{(1)} \tilde{C}_0 + \\
& + m_b \left(m_t H^{(1)} + M^0_\alpha G^{(1)} + m_b A^{(1)} + M_i E^{(1)} \right) C_{12} \\
& + m_t \left(m_t A^{(1)} + M^0_\alpha B^{(1)} + m_b H^{(1)} + M_i D^{(1)} \right) (C_{11} - C_{12}) \\
& + \left(m_t m_b H^{(1)} + m_t M_i D^{(1)} + M^0_\alpha m_b G^{(1)} + M_i M^0_\alpha C^{(1)} \right) C_0 \Big] ,
\end{aligned} \tag{4.56}$$

where the overall coefficients M_L and M_R are the following:

$$M_L = -\frac{ig^2 M_W}{m_b \tan\beta} \qquad M_R = -\frac{ig^2 M_W}{m_t \cot\beta}\,. \tag{4.57}$$

In eq. (4.56) the C-functions must be evaluated with arguments:

$$C_* = C_*\left(p, p', m_{\tilde{t}_a}, M^0_\alpha, M_i\right)\,. \tag{4.58}$$

- Diagram (V_{S2}): For this diagram –which in contrast to the others is finite– we also use the matrices on eqs. (2.31) and (2.34), and introduce the shorthands

$$A^{(b)}_\pm \equiv A^{(b)}_{\pm b\alpha} \quad \text{and} \quad A^{(t)}_\pm \equiv A^{(t)}_{\pm a\alpha}\,,$$

to define the products of coupling matrices

$$\begin{aligned} A^{(2)} &= G_{ba} A^{(b)*}_+ A^{(t)}_-\,, & C^{(2)} &= G_{ba} A^{(b)*}_- A^{(t)}_-\,, \\ B^{(2)} &= G_{ba} A^{(b)*}_+ A^{(t)}_+\,, & D^{(2)} &= G_{ba} A^{(b)*}_- A^{(t)}_+\,. \end{aligned}$$

The contribution to the form factors H_R and H_L from this diagram is

$$\begin{aligned} H_R &= \frac{M_L}{2M_W}\left[m_b B^{(2)} C_{12} + m_t C^{(2)}\left(C_{11} - C_{12}\right) - M^0_\alpha D^{(2)} C_0\right]\,, \\ H_L &= \frac{M_R}{2M_W}\left[m_b C^{(2)} C_{12} + m_t B^{(2)}\left(C_{11} - C_{12}\right) - M^0_\alpha A^{(2)} C_0\right]\,, \end{aligned}$$

the coefficients M_L, M_R being those of eq. (4.57) and the scalar 3-point functions now evaluated with arguments

$$C_* = C_*\left(p, p', M^0_\alpha, m_{\tilde{t}_a}, m_{\tilde{b}_b}\right)\,.$$

- Diagram (V_{S3}): For this diagram we will need

$$A_\pm \equiv A^{(b)}_{\pm ai} \quad \text{and} \quad A^{(0)}_\pm \equiv A^{(b)}_{\pm a\alpha}\,,$$

and again omitting indices we shall use

$$\begin{aligned}
A^{(3)} &= \cos\beta A_+^{(0)*} Q^L A_- \,, & E^{(3)} &= \cos\beta A_-^{(0)*} Q^L A_- \,, \\
B^{(3)} &= \cos\beta A_+^{(0)*} Q^L A_+ \,, & F^{(3)} &= \cos\beta A_-^{(0)*} Q^L A_+ \,, \\
C^{(3)} &= \sin\beta A_+^{(0)*} Q^R A_- \,, & G^{(3)} &= \sin\beta A_-^{(0)*} Q^R A_- \,, \\
D^{(3)} &= \sin\beta A_+^{(0)*} Q^R A_+ \,, & H^{(3)} &= \sin\beta A_-^{(0)*} Q^R A_+ \,.
\end{aligned} \tag{4.59}$$

From these definitions the contribution of diagram (V_{S3}) to the form factors can be obtained by performing the following changes in that of diagram (V_{S1}), eq. (4.56):

- Everywhere in eqs. (4.56) and (4.58) replace $M_i \leftrightarrow M_\alpha^0$ and $m_{\tilde{t}_a} \leftrightarrow m_{\tilde{b}_a}$.
- Replace in eq. (4.56) couplings from (4.55) with those of (4.59).
- Include a global minus sign.

4.4.2 Higgs vertex diagrams

Now we consider the contributions arising from the exchange of virtual Higgs particles and Goldstone bosons in the Feynman gauge, as shown in Fig. 4.13. We write the formula for the form factors by giving the value of the overall coefficient N and the arguments of the corresponding 3-point functions.

- Diagram (V_{H1}):

$$\begin{aligned}
H_R &= N\left[m_b^2(C_{12} - C_0) + m_t^2 \cot^2\beta (C_{11} - C_{12})\right], \\
H_L &= N m_b^2 [C_{12} - C_0 + \tan^2\beta (C_{11} - C_{12})], \\
N &= \mp \frac{ig^2}{2}\left(1 - \frac{\{M_{H^0}^2, M_{h^0}^2\}}{2M_W^2}\right)\frac{\{\cos\alpha, \sin\alpha\}}{\cos\beta}\{\cos(\beta-\alpha), \sin(\beta-\alpha)\}, \\
C_* &= C_*\left(p, p', m_b, M_{H^\pm}, \{M_{H^0}, M_{h^0}\}\right) .
\end{aligned}$$

- Diagram (V_{H2}):

$$\begin{aligned}
H_R &= N\cot\beta[m_t^2(C_{11} - C_{12}) + m_b^2(C_0 - C_{12})], \\
H_L &= N m_b^2 \tan\beta(2C_{12} - C_{11} - C_0),
\end{aligned}$$

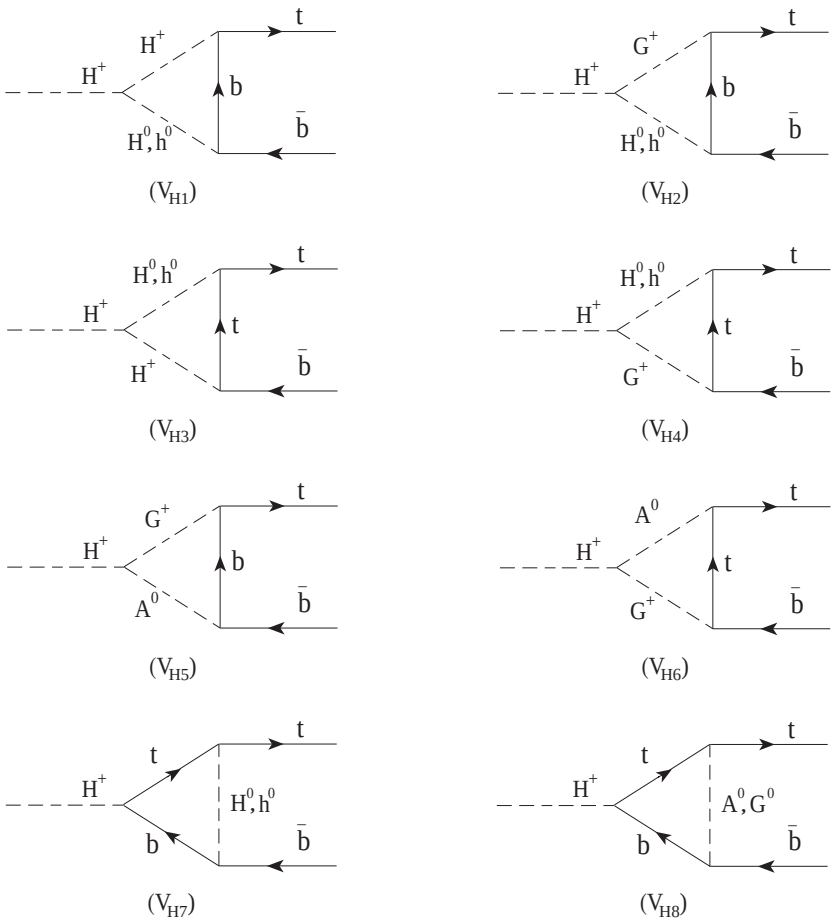

Figure 4.13: *Feynman diagrams, up to one-loop order, for the Higgs and Goldstone boson vertex corrections to the decay process* $H^+ \to t\bar{b}$.

$$
\begin{aligned}
N &= \frac{ig^2}{4}\frac{\{\cos\alpha, \sin\alpha\}}{\cos\beta}\{\sin(\beta-\alpha), \cos(\beta-\alpha)\}\left(\frac{M_{H^\pm}^2}{M_W^2} - \frac{\{M_{H^0}^2, M_{h^0}^2\}}{M_W^2}\right), \\
C_* &= C_*\left(p, p', m_b, M_W, \{M_{H^0}, M_{h^0}\}\right).
\end{aligned}
$$

- Diagram (V_{H3}):

$$
\begin{aligned}
H_R &= N m_t^2[\cot^2\beta C_{12} + C_{11} - C_{12} - C_0], \\
H_L &= N\left[m_b^2 \tan^2\beta C_{12} + m_t^2(C_{11} - C_{12} - C_0)\right], \\
N &= -\frac{ig^2}{2}\frac{\{\sin\alpha, \cos\alpha\}}{\sin\beta}\{\cos(\beta-\alpha), \sin(\beta-\alpha)\}\left(1 - \frac{\{M_{H^0}^2, M_{h^0}^2\}}{2M_W^2}\right), \\
C_* &= C_*\left(p, p', m_t, \{M_{H^0}, M_{h^0}\}, M_{H^\pm}\right).
\end{aligned}
$$

- Diagram (V_{H4}):

$$
\begin{aligned}
H_R &= N m_t^2(2C_{12} - C_{11} + C_0)\cot\beta, \\
H_L &= N\left[-m_b^2 C_{12} + m_t^2(C_{11} - C_{12} - C_0)\right]\tan\beta, \\
N &= \mp\frac{ig^2}{4}\frac{\{\sin\alpha, \cos\alpha\}}{\sin\beta}\{\sin(\beta-\alpha), \cos(\beta-\alpha)\}\left(\frac{M_{H^\pm}^2}{M_W^2} - \frac{\{M_{H^0}^2, M_{h^0}^2\}}{M_W^2}\right), \\
C_* &= C_*\left(p, p', m_t, \{M_{H^0}, M_{h^0}\}, M_W\right).
\end{aligned}
$$

- Diagram (V_{H5}):

$$
\begin{aligned}
H_R &= N\left[m_b^2(C_{12} + C_0) + m_t^2(C_{11} - C_{12})\right], \\
H_L &= N m_b^2 \tan^2\beta(C_{11} + C_0), \\
N &= -\frac{ig^2}{4}\left(\frac{M_{H^\pm}^2}{M_W^2} - \frac{M_{A^0}^2}{M_W^2}\right), \\
C_* &= C_*\left(p, p', m_b, M_W, M_{A^0}\right).
\end{aligned}
$$

- Diagram (V_{H6}):

$$
\begin{aligned}
H_R &= N m_t^2 \cot^2\beta(C_{11} + C_0), \\
H_L &= N\left[m_b^2 C_{12} + m_t^2(C_{11} - C_{12} + C_0)\right], \\
N &= -\frac{ig^2}{4}\left(\frac{M_{H^\pm}^2}{M_W^2} - \frac{M_{A^0}^2}{M_W^2}\right), \\
C_* &= C_*\left(p, p', m_t, M_{A^0}, M_W\right).
\end{aligned}
$$

- Diagram (V_{H7}):

$$\begin{aligned}
H_R &= N \quad [(2m_b^2 C_{11} + \tilde{C}_0 + 2(m_t^2 - m_b^2)(C_{11} - C_{12}))\cot^2\beta \\
&\quad +2m_b^2(C_{11} + 2C_0)]m_t^2\,, \\
H_L &= N \quad [(2m_b^2 C_{11} + \tilde{C}_0 + 2(m_t^2 - m_b^2)(C_{11} - C_{12}))\tan^2\beta \\
&\quad +2m_t^2(C_{11} + 2C_0)]m_b^2\,, \\
N &= \pm\frac{ig^2}{4M_W^2}\frac{\sin\alpha\cos\alpha}{\sin\beta\cos\beta}\,, \\
C_* &= C_*\left(p, p', \{M_{H^0}, M_{h^0}\}, m_t, m_b\right)\,.
\end{aligned}$$

- Diagram (V_{H8}):

$$\begin{aligned}
H_R &= N m_t^2 \cot^2\beta\, \tilde{C}_0\,, \\
H_L &= N m_b^2 \tan^2\beta\, \tilde{C}_0\,, \\
N &= \mp\frac{ig^2}{4M_W^2}\,, \\
C_* &= C_*\left(p, p', \{M_{A^0}, M_Z\}, m_t, m_b\right)\,.
\end{aligned}$$

In the equations above, it is understood that the CP-even mixing angle, α, is renormalized into $\alpha_{\rm eff}$ by the one-loop Higgs mass relations [77–81].

As for the SUSY and Higgs contributions to the counterterms, they are much simpler since they just involve 2-point functions. Thus we shall present the full electroweak results by adding up the various sparticle and Higgs effects. In the following formulae, we append labels referring to the specific diagrams on Figs.4.15-4.17.

4.4.3 Counterterms

- Counterterms $\delta m_f\,, \delta Z_L^f\,, \delta Z_R^f$: For a given down-like fermion b, and corresponding isospin partner t, the fermionic self-energies receive contributions

$$\begin{aligned}
\Sigma^b_{\{L,R\}}(p^2) &= \Sigma^b_{\{L,R\}}(p^2)\Big|_{(C_{b0})+(C_{b1})+(C_{b2})} \\
&= +8\pi\alpha_s C_F \left|R^{(b)}_{\{1,2\}a}\right|^2 [B_1 - B_0]\left(p, m_{\tilde{q}_a}, m_{\tilde{g}}\right)
\end{aligned}$$

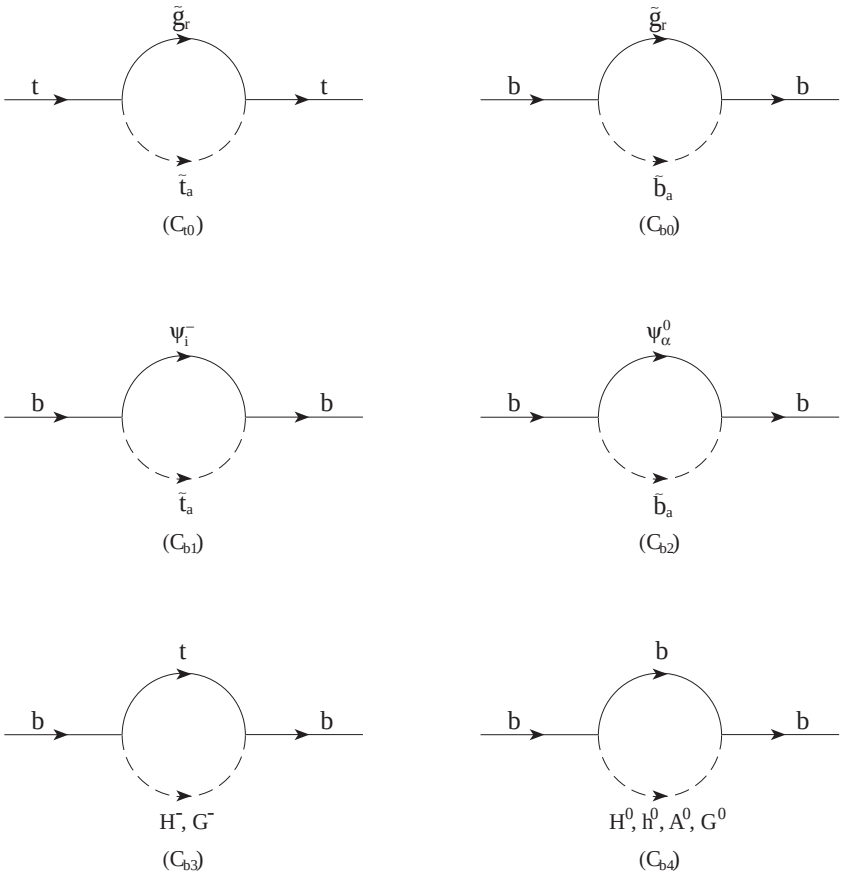

Figure 4.14: *QCD and Electroweak self-energy corrections to the top and bottom quark external lines from the various supersymmetric particles, Higgs and Goldstone bosons. (Cont.)*

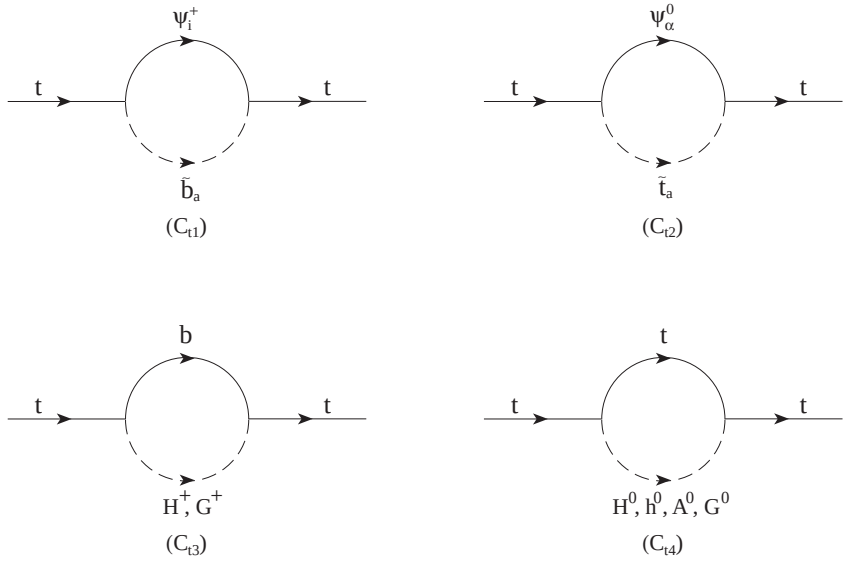

Figure 4.15: *QCD and Electroweak self-energy corrections to the top and bottom quark external lines from the various supersymmetric particles, Higgs and Goldstone bosons. (Cont.)*

$$
\begin{aligned}
& -ig^2 \left[\left| A^{(t)}_{\pm ai} \right|^2 B_1 \left(p, M_i, m_{\tilde{t}_a} \right) \right. \\
& \qquad \left. + \frac{1}{2} \left| A^{(b)}_{\pm a\alpha} \right|^2 B_1 \left(p, M^0_\alpha, m_{\tilde{b}_a} \right) \right] , \qquad (4.60)
\end{aligned}
$$

$$
\begin{aligned}
m_b \Sigma^b_S(p^2) &= m_b \Sigma^b_S(p^2) \Big|_{(C_{b0})+(C_{b1})+(C_{b2})} \\
&= -8\pi\alpha_s C_F \frac{m_{\tilde{g}}}{m_b ?} R^{(b)}_{1a} R^{(b)}_{2a} B_0 \left(p, m_{\tilde{q}_a}, m_{\tilde{g}} \right) \\
&\quad + ig^2 \left[M_i \mathrm{Re} \left(A^{(t)*}_{+ai} A^{(t)}_{-ai} \right) B_0 \left(p, M_i, m_{\tilde{t}_a} \right) \right. \\
&\quad \left. + \frac{1}{2} M^0_\alpha \mathrm{Re} \left(A^{(b)*}_{-a\alpha} A^{(b)}_{+a\alpha} \right) B_0 \left(p, M^0_\alpha, m_{\tilde{b}_a} \right) \right] , \qquad (4.61)
\end{aligned}
$$

from SUSY particles, and

$$
\begin{aligned}
\Sigma^b_{\{L,R\}}(p^2) &= \Sigma^b_{\{L,R\}}(p^2) \Big|_{(C_{b3})+(C_{b4})} \\
&= \frac{g^2}{2iM_W^2} \left\{ m^2_{\{t,b\}} \left[\{\cot^2\beta, \tan^2\beta\} B_1(p, m_t, M_{H^\pm}) \right. \right. \\
&\qquad \left. \left. + B_1(p, m_t, M_W) \right] \right.
\end{aligned}
$$

$$
\begin{aligned}
&+ \frac{m_b^2}{2\cos^2\beta}\Big[\cos^2\alpha\, B_1(p, m_b, M_{H^0}) \\
&\qquad + \sin^2\alpha\, B_1(p, m_b, M_{h^0}) \\
&\qquad + \sin^2\beta\, B_1(p, m_b, M_{A^0}) \\
&\qquad + \cos^2\beta\, B_1(p, m_b, M_Z)\Big]\Big\}\,, \qquad (4.62)
\end{aligned}
$$

$$
\begin{aligned}
\Sigma_S^b(p^2) &= \Sigma_S^b(p^2)\Big|_{(C_{b3})+(C_{b4})} \\
&= -\frac{g^2}{2iM_W^2}\Big\{m_t^2\,[B_0(p, m_t, M_{H^\pm}) - B_0(p, m_t, M_W)] \\
&\qquad + \frac{m_b^2}{2\cos^2\beta}\Big[\cos^2\alpha\, B_0(p, m_b, M_{H^0}) \\
&\qquad\quad + \sin^2\alpha\, B_0(p, m_b, M_{h^0}) \\
&\qquad\quad - \sin^2\beta\, B_0(p, m_b, M_{A^0}) \\
&\qquad\quad - \cos^2\beta\, B_0(p, m_b, M_Z)\Big]\Big\}\,, \qquad (4.63)
\end{aligned}
$$

from Higgs and Goldstone bosons in the Feynman gauge. To obtain the corresponding expressions for an up-like fermion, t, just perform the label substitutions $b \leftrightarrow t$ on eqs. (4.60)-(4.63); and on eqs. (4.62)-(4.63) replace $\sin\alpha \leftrightarrow \cos\alpha$ and $\sin\beta \leftrightarrow \cos\beta$ (which also implies replacing $\tan\beta \leftrightarrow \cot\beta$).

Introducing the above expressions into eqs. (3.27)-(3.27) one immediately obtains the SUSY contribution to the counterterms $\delta m_f\,, \delta Z_{L,R}^f$.

- Counterterm $\delta Z_{H^\pm}$:

$$
\begin{aligned}
\delta Z_{H^\pm} &= \delta Z_{H^\pm}|_{(C_{H1})+(C_{H2})+(C_{H3})+(C_{H4})+(C_{H5})+(C_{H6})} = \Sigma'_{H^\pm}(M_{H^\pm}^2) \\
&= -\frac{ig^2 N_C}{M_W^2}\Big[(m_b^2\tan^2\beta + m_t^2\cot^2\beta)(B_1 + M_{H^\pm}^2 B_1' + m_b^2 B_0') \\
&\qquad + 2m_b^2 m_t^2 B_0'\Big](M_{H^\pm}, m_b, m_t) \\
&\quad + \frac{ig^2}{2M_W^2} N_C \sum_{ab} |G_{ba}|^2\, B_0'(M_{H^\pm}, m_{\tilde{b}_b}, m_{\tilde{t}_a})
\end{aligned}
$$

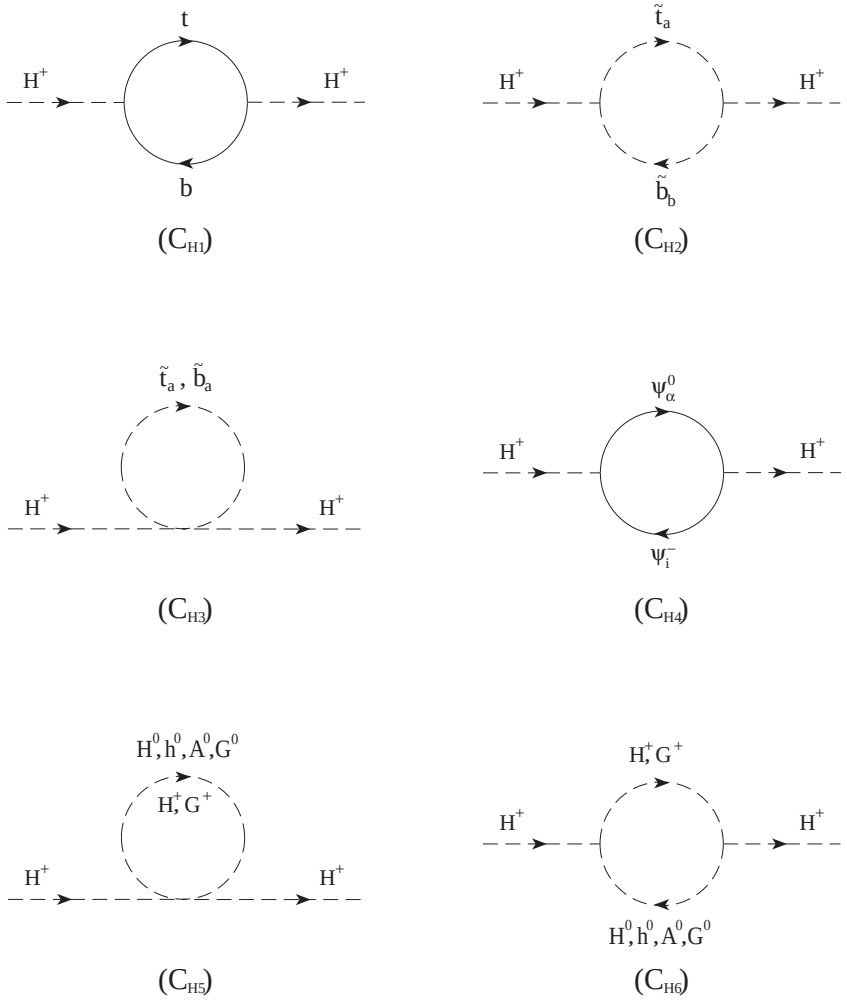

Figure 4.16: *Corrections to the charged Higgs self-energy from the various supersymmetric particles and matter fermions. Only the third quark-squark generation is illustrated.*

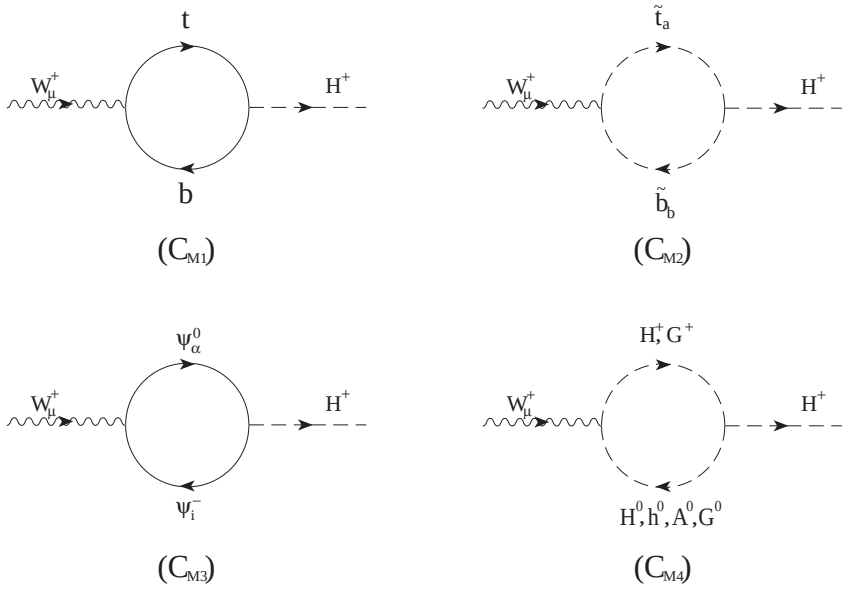

Figure 4.17: *Corrections to the mixed $W^+ - H^+$ self-energy from the various supersymmetric particles and matter fermions. Only the third quark-squark generation is illustrated.*

$$
\begin{aligned}
&-2ig^2 \sum_{i\alpha} \left[\left(\left| Q^L_{\alpha i} \right|^2 \cos^2\beta + \left| Q^R_{\alpha i} \right|^2 \sin^2\beta \right) \left(B_1 + M^2_{H^\pm} B'_1 + M^{0\,2}_\alpha B'_0 \right) \right. \\
&\qquad \left. + 2M_i M^0_\alpha Re\left(Q^L_{\alpha i} Q^{R*}_{\alpha i} \right) \sin\beta\cos\beta B'_0 \right] \left(M_{H^\pm}, M^0_\alpha, M_i \right) \\
&+ig^2 \sum_{AB} \left| M^{H^+}_{AB} \right|^2 B'_0(M_{H^\pm}, m_{H_A}, m_{H_B}) \,. \qquad (4.64)
\end{aligned}
$$

where m_{H_A} is either the charged Higgs mass or the charged Goldstone mass (m_{W^+} and m_{H_B} is one of neutral Higgses or the Neutral Goldstone mass (m_Z) (Cf. eq. 2.8). Notice that diagrams (C_{H3}) and (C_{H5}) give a vanishing contribution to $\delta Z_{H^\pm}$.

- Counterterm δZ_{HW}:

$$
\begin{aligned}
\delta Z_{HW} &= \delta Z_{HW}|_{(C_{M1})+(C_{M2})+(C_{M3})} = \frac{\Sigma_{HW}(M^2_{H^\pm})}{M^2_W} \\
&= -\frac{ig^2 N_C}{M^2_W} \left[m^2_b \tan\beta (B_0 + B_1) + m^2_t \cot\beta B_1 \right] (M_{H^\pm}, m_b, m_t) \\
&\quad -\frac{ig^2 N_C}{2M^2_W} \sum_{ab} G_{ba} R^{(t)}_{1a} R^{(b)*}_{1b} \left[2B_1 + B_0 \right] (M_{H^\pm}, m_{\tilde{b}_b}, m_{\tilde{t}_a})
\end{aligned}
$$

$$+\frac{2ig^2}{M_W}\sum_{i\alpha}\Big[M^0_\alpha\left(\cos\beta\; Q^{L*}_{\alpha i}C^L_{\alpha i}+\sin\beta\; Q^{R*}_{\alpha i}C^R_{\alpha i}\right)(B_0+B_1)$$
$$+\,M_i\left(\sin\beta\; Q^{R*}_{\alpha i}C^L_{\alpha i}+\cos\beta\; Q^{L*}_{\alpha i}C^R_{\alpha i}\right)B_1\Big](M_{H^\pm},M^0_\alpha,M_i)$$
$$-ig^2\sum_{AB}M^{H^+}_{AB}M^{W^+}_{AB}\,[2B_1+B_0]\,(M_{H^\pm},m_{H_A},m_{H_B})\,. \qquad (4.65)$$

where a sum is understood over all generations and we have defined:

$$\begin{aligned}
M^{W^+}_{H^+\{H_0,h_0\}} &= -\frac{\{\sin(\alpha-\beta),\,\cos(\alpha-\beta)\}}{2}\\
M^{W^+}_{H^+\{A_0,G_0\}} &= \{\frac{i}{2},\,0\}\\
M^{W^+}_{G^+\{H_0,h_0\}} &= -\frac{\{\cos(\beta-\alpha),\,\sin(\beta-\alpha)\}}{2}\\
M^{W^+}_{G^+\{A_0,G_0\}} &= \{0,\,\frac{i}{2}\}
\end{aligned} \qquad (4.66)$$

Finally, the evaluation of Δ_τ on eq.(4.48) yields similar bulky analytical formulae, which follow after computing diagrams akin to those in Figs.4.12-4.17 for the MSSM corrections to $H^+\to\tau^+\nu_\tau$. We refrain from quoting them explicitly here. The numerical effect, though, will be explicitly given in the next section (4.5).

4.4.4 Analytical results

We are now ready to furnish the corrected width of $H^+\to t\bar{b}$ in the MSSM. It just follows after computing the interference between the tree-level amplitude and the one-loop amplitude. It is convenient to express the result as a relative correction with respect to the tree-level width both in the α-scheme and in the G_F-scheme. In the former we obtain the relative MSSM correction

$$\begin{aligned}
\delta^{MSSM}_\alpha &= \frac{\Gamma-\Gamma^{(0)}_\alpha}{\Gamma^{(0)}_\alpha}\\
&= \frac{N_L}{D}\,[2\,Re(G_L)]+\frac{N_R}{D}\,[2\,Re(G_R)]+\frac{N_{LR}}{D}\,[2\,Re(G_L+G_R)]\,,
\end{aligned} \qquad (4.67)$$

where the corresponding lowest-order width was defined in 4.2 and

$$D = (M^2_{H^\pm}-m_t^2-m_b^2)\,(m_t^2\cot^2\beta+m_b^2\tan^2\beta)-4m_t^2m_b^2\,,$$

$$\begin{aligned} N_R &= (M_{H^\pm}^2 - m_t^2 - m_b^2)\, m_b^2 \tan^2\beta\,, \\ N_L &= (M_{H^\pm}^2 - m_t^2 - m_b^2)\, m_t^2 \cot^2\beta\,, \\ N_{LR} &= -2 m_t^2 m_b^2\,. \end{aligned} \tag{4.68}$$

From these equations it is obvious that at low $\tan\beta$ the relevant quantum effects basically come from the contributions to the form factor G_L whereas at high $\tan\beta$ they come from G_R.

Using eq.(3.29) we find that the relative MSSM correction in the G_F-parametrization reads

$$\delta_{G_F}^{MSSM} = \frac{\Gamma - \Gamma_{G_F}^{(0)}}{\Gamma_{G_F}^{(0)}} = \delta_\alpha^{MSSM} - \Delta r^{MSSM}\,, \tag{4.69}$$

where the tree-level width in the G_F-scheme, $\Gamma_{G_F}^{(0)}$, is given by eq.(4.3) and is related to eq.(4.2) through

$$\Gamma_\alpha^{(0)} = \Gamma_{G_F}^{(0)}\,(1 - \Delta r^{MSSM})\,. \tag{4.70}$$

Before presenting the results of the complete numerical analysis, it should be clear that the bulk of the high $\tan\beta$ corrections to the decay rate of $H^+ \to t\bar{b}$ in the MSSM is expected to come from SUSY-QCD. This could already be foreseen from what is known in SUSY GUT models [133, 134, 149]; in fact, in this context a non-vanishing sbottom mixing (which we also assume in our analysis) may lead to important SUSY-QCD quantum effects on the bottom mass, $m_b = m_b^{GUT} + \Delta m_b$, where Δm_b is proportional to $M_{LR}^b \to -\mu \tan\beta$ at sufficiently high $\tan\beta$. These are finite threshold effects that one has to include when matching the SM and MSSM renormalization group equations (RGE) at the effective supersymmetric threshold scale, T_{SUSY}, above which the RGE evolve according to the MSSM β-functions in the $\overline{MS}$ scheme [150]. In our case, since the bottom mass is an input parameter for the on-shell scheme, these effects obviously have a different physical meaning, but are formally the same; they are just fed into the mass counterterm $\delta m_b/m_b$ on eq.(4.53) and contribute to it with opposite sign ($\delta m_b/m_b = -\Delta m_b + ...$) [3].

[3] In the alternative framework of Ref. [151], the SUSY-QCD corrections have been computed assuming no mixing in the sbottom mass matrix. Nonetheless, the typical size of the SUSY-QCD corrections does not

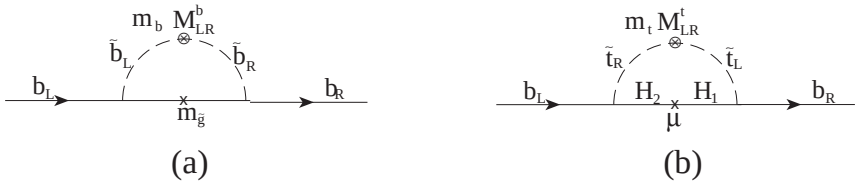

Figure 4.18: *(a) Leading SUSY-QCD contributions to $\delta m_b/m_b$ in the electroweak-eigenstate basis; (b) Leading supersymmetric Yukawa coupling contributions to $\delta m_b/m_b$ in the electroweak-eigenstate basis.*

Explicitly, when viewed in terms of diagrams of the electroweak eigenstate basis, the relevant finite corrections from the bottom mass counterterm are generated by mixed LR-sbottoms and gluino loops (Cf. Fig.4.18a):

$$\left(\frac{\delta m_b}{m_b}\right)_{\rm SUSY-QCD} = \frac{2\alpha_s(m_t)}{3\pi}\, m_{\tilde{g}}\, M^b_{LR}\, I(m_{\tilde{b}_1}, m_{\tilde{b}_2}, m_{\tilde{g}})$$
$$\to -\frac{2\alpha_s(m_t)}{3\pi}\, m_{\tilde{g}}\, \mu \tan\beta\, I(m_{\tilde{b}_1}, m_{\tilde{b}_2}, m_{\tilde{g}})\,, \qquad (4.71)$$

where the last result holds for sufficiently large $\tan\beta$ and for μ not too small as compared to A_b. We have introduced the positive-definite function (Cf. Appendix A)

$$I(m_1, m_2, m_3) \equiv 16\,\pi^2\, i\, C_0(0, 0, m_1, m_2, m_3)$$
$$= \frac{m_1^2\, m_2^2 \ln\frac{m_1^2}{m_2^2} + m_2^2\, m_3^2 \ln\frac{m_2^2}{m_3^2} + m_1^2\, m_3^2 \ln\frac{m_3^2}{m_1^2}}{(m_1^2 - m_2^2)\,(m_2^2 - m_3^2)\,(m_1^2 - m_3^2)}\,. \qquad (4.72)$$

In addition, we could also foresee potentially large (finite) SUSY electroweak effects from $\delta m_b/m_b$. They are induced by $\tan\beta$-enhanced Yukawa couplings of the type (2.5). Of course, these effects have already been fully included in the calculation presented in Section 4.5 that we have performed in the mass-eigenstate basis, but it is illustrative of the origin of the leading contributions to pick them up again directly from the diagrams in the electroweak-eigenstate

change as compared to the present approach (in which we do assume a non-diagonal sbottom matrix) the reason being that in the absence of sbottom mixing, i.e. $M^b_{LR} = 0$, the contribution $\delta m_b/m_b \propto -\mu\tan\beta$ at large $\tan\beta$ is no longer possible but, in contrast, the vertex correction does precisely inherits this dependence and compensates for it. The drawback of an scenario based on $M^b_{LR} = 0$, however, is that when it is combined with a large value of $\tan\beta$ it may lead to a value of A_b which overshoots the natural range expected for this parameter.

basis. In this case, from loops involving mixed LR-stops and mixed charged higgsinos (Cf. Fig.4.18b), one finds:

$$\left(\frac{\delta m_b}{m_b}\right)_{\rm SUSY-Yukawa} = -\frac{h_t\, h_b}{16\pi^2}\,\frac{\mu}{m_b}\, m_t\, M^t_{LR} I(m_{\tilde{t}_1}, m_{\tilde{t}_2}, \mu)$$
$$\to -\frac{h_t^2}{16\pi^2}\,\mu \tan\beta\, A_t\, I(m_{\tilde{t}_1}, m_{\tilde{t}_2}, \mu)\,, \qquad (4.73)$$

where again the last expression holds for large enough $\tan\beta$.

Notice that, at variance with eq.(4.71), the Yukawa coupling correction (4.73) dies away with increasing μ. Setting $h_t \simeq 1$ at high $\tan\beta$, and assuming that there is no large hierarchy between the sparticle masses, the ratio between (4.71) and (4.73) is given, in good approximation, by $4\, m_{\tilde{g}}/A_t$ times a slowly varying function of the masses of order 1, where the (approximate) proportionality to the gluino mass reflects the very slow decoupling rate of the latter [151].

In view of the present bounds on the gluino mass, and since A_t (as well as A_b) cannot increase arbitrarily –as also noted above– we expect that the SUSY-QCD effects can be dominant, and even overwhelming for sufficiently heavy gluinos. Unfortunately, in contradistinction to the SUSY-QCD case, there are also plenty of additional vertex contributions both from the Higgs sector and from the stop-sbottom/gaugino-higgsino sector where those Yukawa couplings do enter the game. So if one wishes to trace the origin of the leading contributions in the electroweak-eigenstate basis, a similar though somewhat more involved exercise has to be carried out also for vertex functions. Of course, all of these effects are fully included in our calculation of Section 4.4 within the framework of the mass-eigenstate basis[4].

A few words are in order about these *finite threshold effects* coming from diagrams in Fig 4.18. As explained early, formally, eq.(4.71) describes the same one-loop *threshold effect* from massive particles that one has to introduce to correct the ordinary massless contributions (i.e. to correct the standard QCD running bottom quark mass) in SUSY GUT models

[4]The mass-eigenstate basis is extremely convenient to carry out the numerical analysis, but it does not immediately provide a "physical interpretation" of the results. The electroweak-eigenstate basis, in contrast, is a better bookkeeping device to trace the origin of the most relevant effects, but as a drawback the intricacies of the full analytical calculation can be abhorrent.

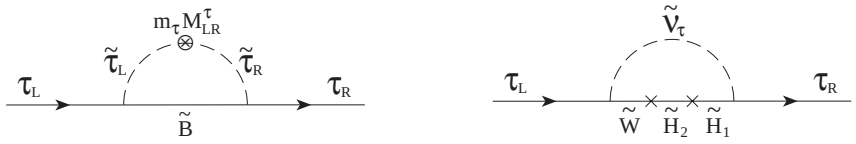

Figure 4.19: *Leading supersymmetric electroweak contributions to $\delta m_\tau/m_\tau$ in the electroweak-eigenstate basis.*

[129, 133, 134]. In fact their contribution is finite and *non-decoupling*, that is, if you scale up all the SUSY parameters (i.e. $m_{\tilde{g}}$, $m_{\tilde{b}_a}$, $m_{\tilde{t}_b}$, A_t, μ) by a factor λ the contributions described in eqs. 4.71 and 4.73 remain invariant!. However, if one scales up all supersymmetric parameters a non trivial fine-tuning would be needed to allow for a relatively light –around 250 GeV– charged Higgs, so in this it is unnatural. Notice that in the absence of SUSY-breaking terms ($m_{\tilde{g}} = 0$, $A_t = 0$) these non-decoupling effects exactly vanish. So, their origin is the SUSY-breaking sector. In the SUSY-QCD contribution (eq. 4.71), it is specially clear that the non-decoupling can be achieved by increasing physical parameters, namely the gluino, squark and higgsino masses. In fact, one may increase the chargino mass by letting $\mu \to \infty$ without decreasing the other masses, which may be allowed to grow independently.

The main source of process-dependent δ_τ-effects lies in the corrections generated by the τ-mass counterterm, $\delta m_\tau/m_\tau$, and can be easily picked out in the electroweak-eigenstate basis (see Fig.4.19) much in the same way as we did for the b-mass counterterm. There are, however, some differences, as can be appraised by comparing the diagrams in Figs.4.18 and 4.19, where we see that in the latter case the effect derives from diagrams involving τ-sleptons with gauginos or mixed gaugino-higgsinos. An explicit computation of the diagrams (a) + (b) in Fig.4.19 yields

$$\begin{aligned} \frac{\delta m_\tau}{m_\tau} &= \frac{g'^2}{16\pi^2}\,\mu\, M'\,\tan\beta\, I(m_{\tilde{\tau}_1}, m_{\tilde{\tau}_2}, M') \\ &+ \frac{g^2}{16\pi^2}\,\mu\, M\,\tan\beta\, I(\mu, m_{\tilde{\nu}_\tau}, M)\,, \end{aligned} \tag{4.74}$$

where $g' = g\, s_W/c_W$ and M', M (Cf. section 2.2.1) are the soft SUSY-breaking Majorana masses associated to the bino $\tilde{B}$ and winos $\tilde{W}^\pm$, respectively, and the function $I(m_1, m_2, m_3)$

is again given by eq.(4.72). In the formula above we have projected, from the bino diagram in Fig.4.19a, only the leading piece which is proportional to $\tan\beta$. Even so, the contribution from the wino-higgsino diagram in Fig.4.19b is much larger. Numerical evaluation of the sum of the two contributions on eq.(4.74) indeed shows that it reproduces to within few percent the full numerical result previously obtained in the mass-eigenstate basis, thus confirming that eq.(4.74) gives the leading contribution. In practice, for a typical choice of parameters, this contribution is approximately cancelled out by part of the electroweak supersymmetric corrections associated to the original process $H^+ \to t\bar{b}$, and one is effectively left with eq.(4.73) as being the main source of electroweak supersymmetric quantum effects at high $\tan\beta$.

As for the standard QCD corrections we use the full analytical formulae of Ref. [116, 117] [5]. In the limit $M_{H^+} \gg m_t$, the standard QCD correction boils down to the simple expression

$$\begin{aligned}\delta_g^{QCD} &= \frac{\Gamma_{QCD} - \Gamma_0}{\Gamma_0} \\ &= \left(\frac{C_F\,\alpha_s}{2\,\pi}\right) \frac{m_t^2\,\cot^2\beta\,\left(\frac{9}{2} - 6\,\log\frac{M_{H^+}}{m_t}\right) + m_b^2\,\tan^2\beta\,\left(\frac{9}{2} - 6\,\log\frac{M_{H^+}}{m_b}\right)}{m_t^2\,\cot^2\beta + m_b^2\,\tan^2\beta}\,. \quad (4.75)\end{aligned}$$

This formula is very convenient to understand the asymptotic behaviour. However, as we have checked, it is inaccurate for the present range of values of m_t unless M_{H^+} is extremely large (beyond $1\,TeV$).

4.5 Numerical analysis and discussion

We may now pass on to the numerical analysis of the over-all quantum effects. After explicit computation of the various loop diagrams, the results are conveniently cast in terms of the relative correction with respect to the tree-level width defined in eq.4.2. In what follows we understand that $\delta \equiv \delta_\alpha$ –Cf. eq.(4.67)– i.e. we shall always give our corrections with respect to the tree-level width Γ_α^0 in the α-scheme. The corresponding correction with respect to the tree-level width in the G_F-scheme is simply given by eq.(4.69), where Δr^{MSSM} was object of a particular study in [111, 112] and therefore it can be easily incorporated, if necessary. Notice,

[5] We have corrected several misprints on eq.(5.2) of Ref. [116, 117].

however, that Δr^{MSSM} is already tightly bound by the experimental data on $M_Z = 91.1863 \pm 0.0020\, GeV$ at LEP and the ratio M_W/M_Z in $p\bar{p}$, which lead to $M_W = 80.356 \pm 0.125\, GeV$. Therefore, even without doing the exact theoretical calculation of Δr within the MSSM, we already know from

$$\Delta r = 1 - \frac{\pi\alpha}{\sqrt{2}\, G_F}\, \frac{1}{M_W^2\,(1 - M_W^2/M_Z^2)}\,, \tag{4.76}$$

that Δr^{MSSM} must lie in the experimental interval $\Delta r^{\rm exp} \simeq 0.040 \pm 0.018$.

Now, since the corrections computed in Section 4.5 can typically be about one order of magnitude larger than Δr (see bellow), the bulk of the quantum effects on $H^+ \to t\bar{b}$ is already comprised in the relative correction (4.67) in the α-scheme. Furthermore, in the conditions under study, only a small fraction of Δr^{MSSM} is supersymmetric [111,112], and we should not be dependent on isolating this universal, relatively small, part of the total SUSY correction to δ. To put in a nutshell: if there is to be any hope to measure supersymmetric quantum effects on the charged Higgs decay of the top quark, they should better come from the potentially large, non-oblique, corrections computed in Section 4.4. The SUSY effects contained in Δr^{MSSM} [111, 112], instead, will be measured in a much more efficient way from a high precision ($\delta M_W^{\rm exp} = \pm 40\, MeV$) determination of M_W at LEP 200 and at the Tevatron.

Even though we shall explore the evolution of our results as a function of the charged Higgs mass in the LHC range, for the numerical analysis we wish to single out the Tevatron accessible window (eq. 4.9)

$$m_t \lesssim M_H \lesssim 300\, GeV\,.$$

In Figs.4.20-4.25 we display in a nutshell our results for a representative choice of parameters within this framework, exhibiting the evolution of the quantum corrections with respect to the tree-level width (4.2), δ^{MSSM}, as a function of the most significant parameters. The MSSM correction (4.67) includes the full QCD yield (both from gluon and gluinos) at $\mathcal{O}(\alpha_s)$ plus all the leading MSSM electroweak effects driven by the Yukawa couplings (2.5). We have defined $\alpha_s = \alpha_s(M_{H^+})$ by means of the (one-loop) expression

$$\alpha_s(M_{H^+}) = \frac{6\,\pi}{(33 - 2\,n_f)\log\left(M_{H^+}/\Lambda_{n_f}\right)}\,, \tag{4.77}$$

normalized as $\alpha_s(M_Z) \simeq 0.12$, where n_f is the number of quark flavors with threshold below the Higgs boson mass M_{H^+}. The rest of the input parameters have already been defined in section 2.2.1

First we will give the known results on the $\widetilde{\text{QCD}}$ corrections [40] to make evident that the $\widetilde{\text{QCD}}$ contribution alone to (δ_g) can be comparable or even larger than the conventional QCD corrections (δ_g). There it is shown, as can also be seen in Figs 4.24a-b, that for a given $\tan\beta$, the relative size of the SUSY-QCD effects versus the standard QCD effects depends on the value of M_{H^+} as can be seen from . Notwithstanding, it is clear that δ_g remains fairly insensitive to M_{H^+}.

The huge experimental impact on the measurement of the $\widetilde{\text{QCD}}$ corrected $\Gamma(H^+ \to t\bar{b})$ is shown in Fig.4.20 where we plot the SUSY-QCD corrected width versus $\tan\beta$, for fixed values of the other parameters. For completeness, we have included in this figure the partial widths of the alternative decays $H^+ \to \tau^+\,\nu_\tau$ and $H^+ \to W^+\,h^0$, which are obviously free of $\mathcal{O}(\alpha_s)$ QCD corrections. (To avoid cluttering, we have not included $H^+ \to c\,\bar{s}$; it is overwhelmed by the τ-lepton mode as soon as $\tan\beta \gtrsim 2$.) It is patent from Fig.4.20 that, for charged Higgs masses above the $t\,\bar{b}$ threshold, the decay $H^+ \to t\,\bar{b}$ is dominant. Only for very large $\tan\beta$ (> 30) and for sufficiently big and positive μ $(\mu > 100\,GeV)$ the negative corrections to $H^+ \to t\,\bar{b}$ are huge enough to drive its partial width down to the level of $H^+ \to \tau^+\,\nu_\tau$. Therefore the top quark decay of the charged Higgs is, by far, the most relevant decay mode to look at.

As already seen in eq. 4.71, depicted in Fig.4.20 and further shown in Figs.4.23a-4.25a the $\widetilde{\text{QCD}}$ contribution is extremely sensitive to μ both on its value and on its sign. It turns out that the sign of the SUSY-QCD correction is basically opposite to the sign of μ, and the respective corrections for $+\mu$ and for $-\mu$ take on approximately the same absolute value.

At large $\tan\beta$, the role played by the bottom quark mass becomes very important. Indeed, in Fig.4.21 we confirm (in the particular case of $\widetilde{\text{QCD}}$, though it happens similarly for the $\widetilde{\text{EW}}$ effects) that the external self-energies (basically the one from the b-line) give the bulk of the corrections displayed, whereas the (finite) vertex effect is comparatively much smaller and its yield becomes rapidly saturated.

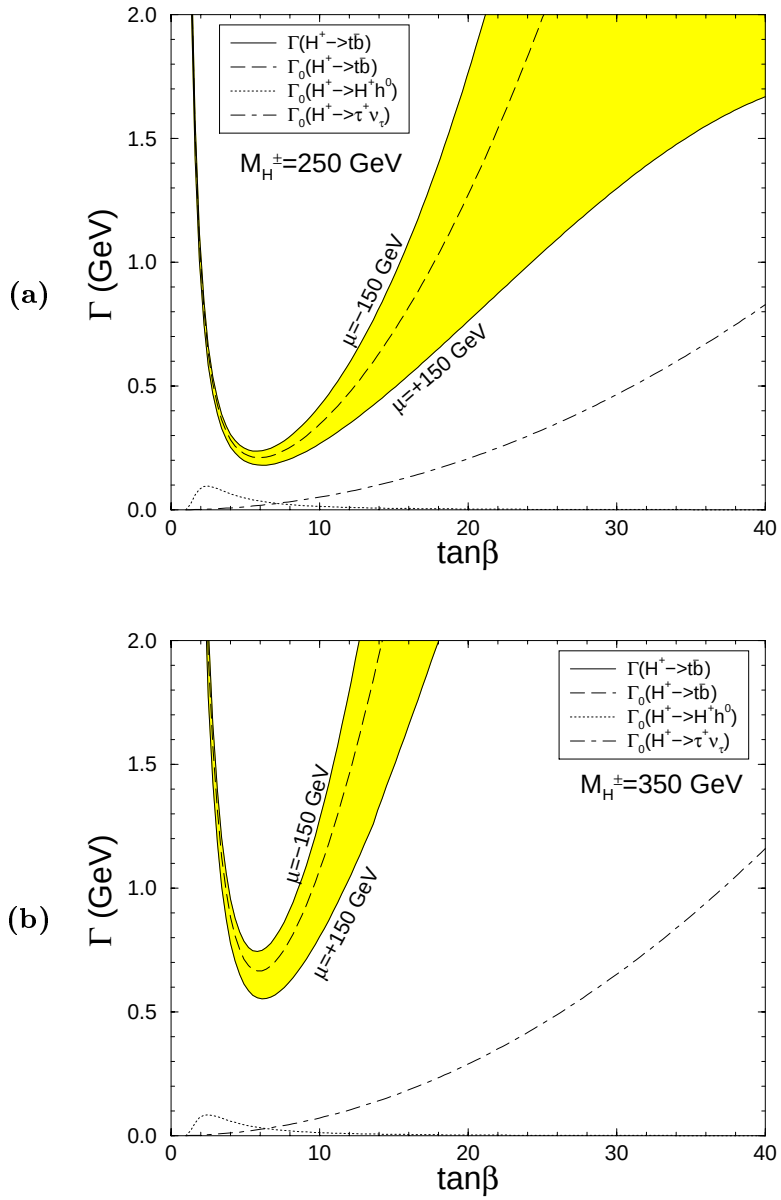

Figure 4.20: *SUSY-QCD corrected* $\Gamma(H^+ \to t\bar{b})$ *as a function of* $\tan\beta$ *for two opposite values of* μ*, compared to the corresponding tree-level width,* $\Gamma_0(H^+ \to t\bar{b})$*; For completeness we have included in this figure the partial widths of the alternative decays* $H^+ \to \tau^+\nu_\tau$ *and* $H^+ \to W^+h^0$*, which are obviously free of* $\mathcal{O}(\alpha_s)$ *QCD corrections. We study these effects in two different Higgs mass scenarios: (a)* $M_{H^\pm} = 250\,\mathrm{GeV}$ *and (b)* $M_{H^\pm} = 350\,\mathrm{GeV}$*.*

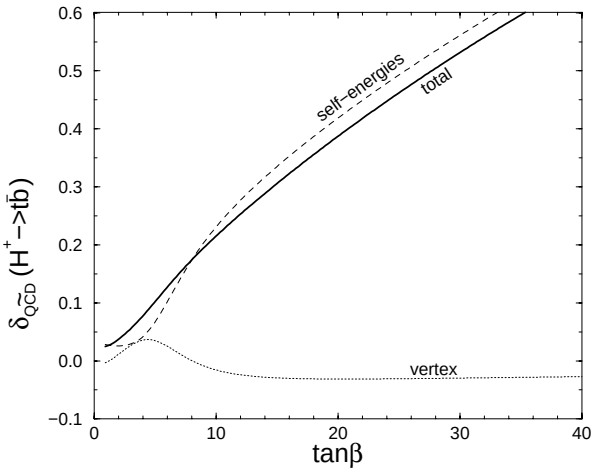

Figure 4.21: *We separate the contributions from vertex and self-energies on the dependence of δ for the $\widetilde{\text{QCD}}$ correction. The self-energy contribution is dominated by the finite threshold effect (eq. 4.71)*

Before continuing we want to stress again that the $\widetilde{\text{QCD}}$ contribution is in most of the MSSM parameter space the leading contribution.

We are now ready to restrict our analysis of $H^+ \to t\,\bar{b}$ including all the SUSY effects ($\widetilde{\text{QCD}}$ and $\widetilde{\text{EW}}$) within the appropriate phenomenological domain pinpointed in Figs.4.5-4.9 which accommodate for different experimental constraints as explained in section. 4.2.

We set out by looking at the branching ratio of $H^+ \to \tau^+\,\nu_\tau$ (Cf. Fig.4.22). Even though the partial width of this process does not get renormalized (as it is used to define $\tan\beta$), its branching ratio is seen to be very much sensitive to the MSSM corrections to $\Gamma(H^+ \to t\,\bar{b})$. For large $\tan\beta$ as in eq.(4.10), $BR(H^+ \to \tau^+\nu_\tau)$ may achieve rather high values $(10 - 50\%)$ for Higgs masses in the interval (4.9), and it never decreases below the $5 - 10\%$ level in the whole range. Therefore, a handle for $\tan\beta$ measurement is always available from the Higgs τ-channel and so also an opportunity for discovering quantum SUSY signatures on $\Gamma(H^+ \to t\,\bar{b})$. As for the other $H^\pm$-decays, we note that the potentially important mode $H^+ \to \tilde{t}_i\,\bar{\tilde{b}}_j$ [152] does not play any role in our case since (for reasons to be clear below) we are mainly led to consider bottom-squarks heavier than the charged Higgs. Moreover, the $H^+ \to W^+\,h^0$ decay which is sizable enough at low $\tan\beta$ becomes extremely depleted at

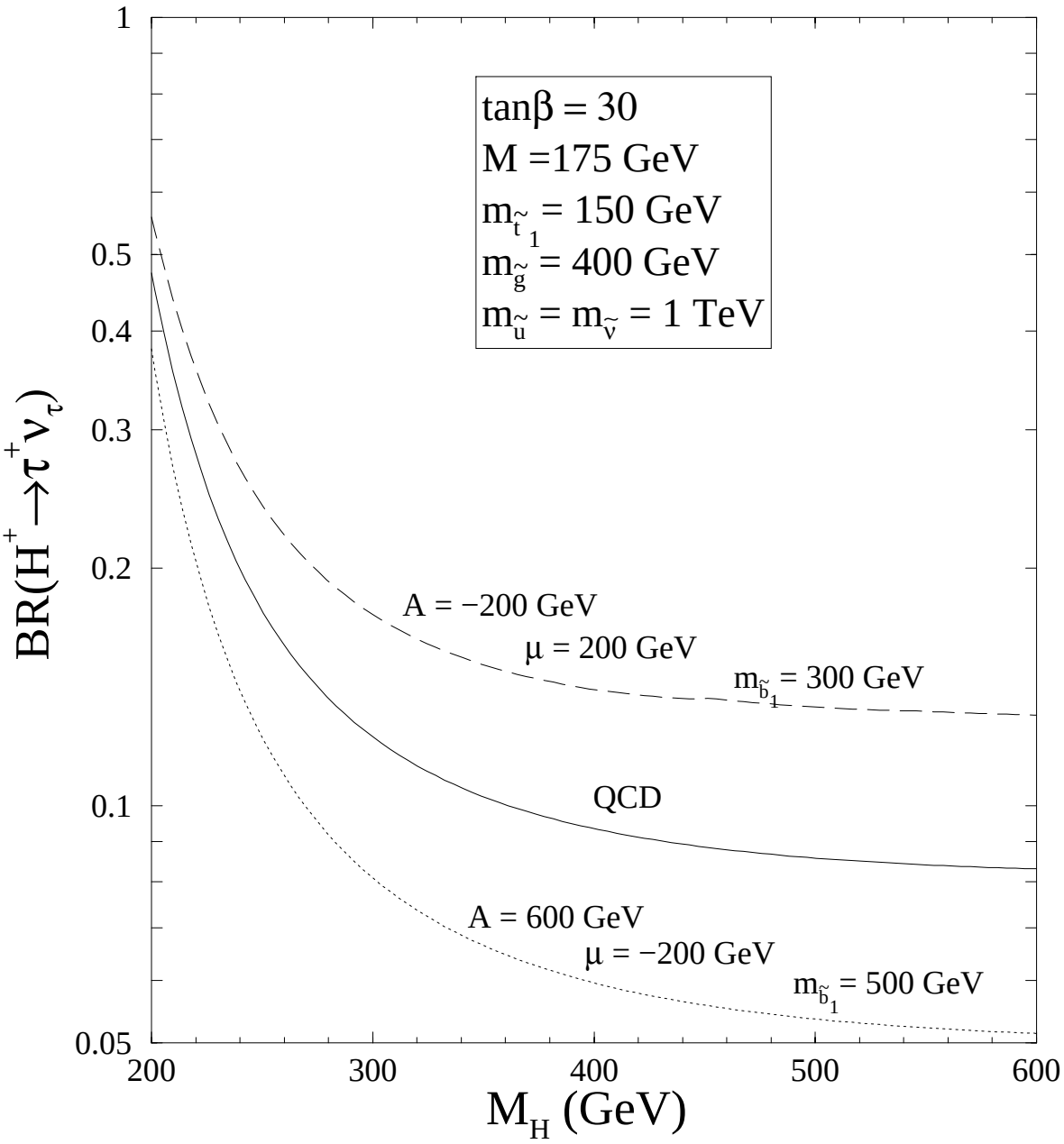

Figure 4.22: *The branching ratio of $H^+ \to \tau^+ \nu_\tau$ for positive and negative values of μ and A_t allowed by eq.(4.4), as a function of the charged Higgs mass; A is a common value for the trilinear couplings. The central curve includes the standard QCD effects only.*

high $\tan\beta$ [40]. Finally, the decays into charginos and neutralinos, $H^+ \to \chi_i^+ \chi_\alpha^0$, are not $\tan\beta$-enhanced and remain negligible. Thus at the end of the day we do find an scenario where $H^+ \to t\,\bar{b}$ and $H^+ \to \tau^+ \nu_\tau$ can be deemed as the only relevant decay modes.

In order to assess the impact of the electroweak effects, we demonstrate that a typical set of inputs can be chosen such that the SUSY-QCD and SUSY-EW outputs are of comparable size.

In Figs.4.23a-4.23b we display δ, eq.(4.67), as a function respectively of $\mu < 0$ and $\tan\beta$ for fixed values of the other parameters (within the $b \to s\,\gamma$ allowed region). Remarkably, in spite of the fact that all sparticle masses are beyond the scope of LEP 200 the corrections are fairly large. We have individually plot the SUSY-EW, SUSY-QCD, standard QCD and total MSSM effects. The Higgs-Goldstone boson corrections (which we have computed in the Feynman gauge) are isolated only in Fig.4.23b just to make clear that they add up non-trivially to a very tiny value in the whole range (4.10), and only in the small corner $\tan\beta < 1$ they can be of some significance.

In Figs.4.23c-4.23d we render the various corrections (4.67) as a function of the relevant squark masses. For $m_{\tilde{b}_1} \lesssim 200\,GeV$ we observe (Cf. Fig.4.23c) that the SUSY-EW contribution is non-negligible ($\delta_{SUSY-EW} \simeq +20\%$) but the SUSY-QCD loops induced by squarks and gluinos are by far the leading SUSY effects ($\delta_{SUSY-QCD} > 50\%$) – the standard QCD correction staying invariable over -20% and the standard EW correction (not shown) being negligible. In contrast, for larger and larger $m_{\tilde{b}_1} > 300\,GeV$, say $m_{\tilde{b}_1} = 400$ or $500\,GeV$, and fixed stop mass at a moderate value $m_{\tilde{t}_1} = 150\,GeV$, the SUSY-EW output is longly sustained whereas the SUSY-QCD one steadily goes down. However, the total SUSY pay-off adds up to about $+40\%$ and the net MSSM yield still reaches a level around $+20\%$, i.e. of equal value but opposite in sign to the conventional QCD result. This would certainly entail a qualitatively distinct quantum signature.

We stress that the main parameter to decouple the SUSY-QCD correction is the lightest sbottom mass, rather than the the gluino mass [40], with which the decoupling is very slow (Fig. 4.24), a fact that indeed has an obvious phenomenological interest. For this reason, since we wished to probe the regions of parameter space where these electroweak effects are

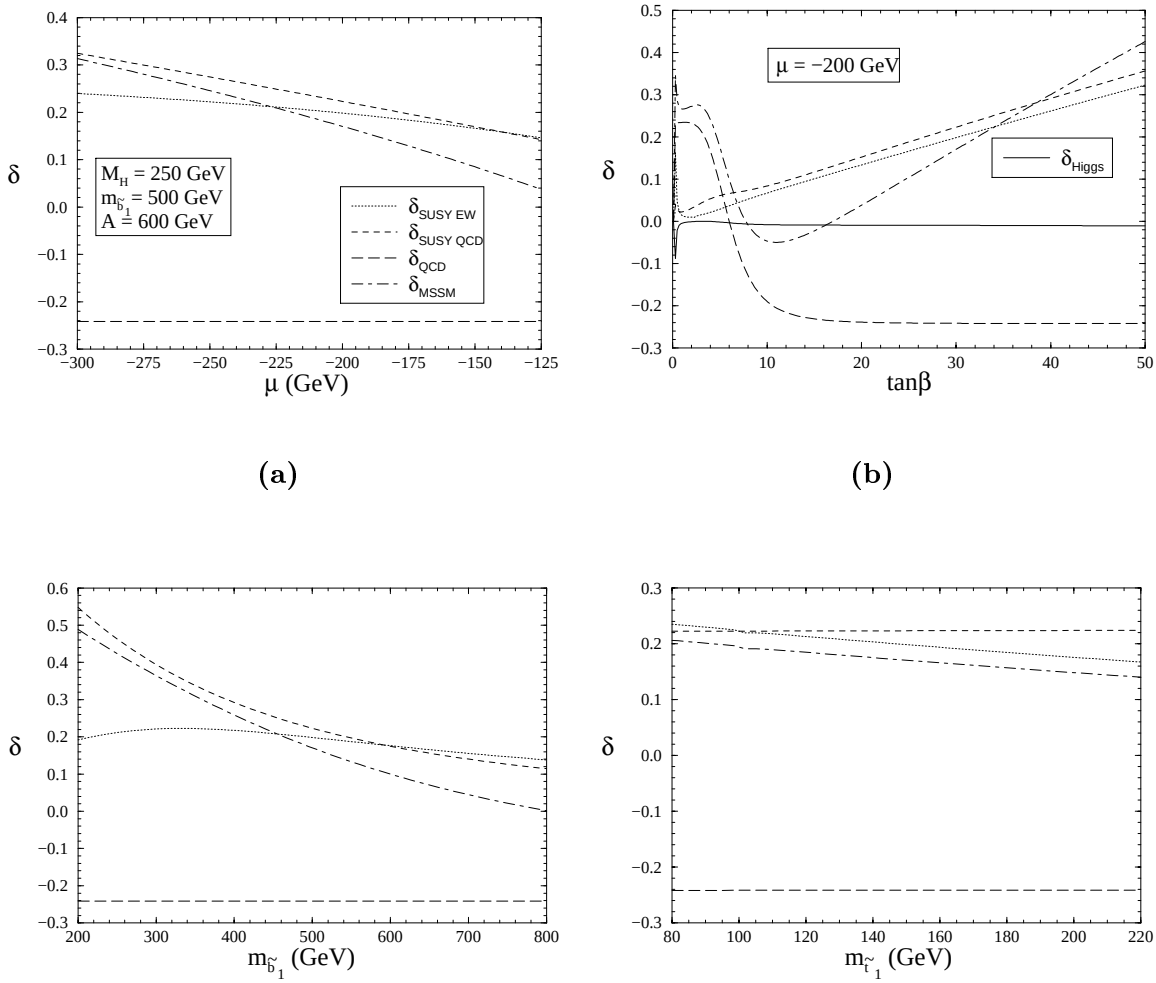

(a) **(b)**

(c) **(d)**

Figure 4.23: *The SUSY-EW, SUSY-QCD, standard QCD and full MSSM contributions to δ, eq.(5.6), as a function of μ;* **(b)** *As in (a), but as a function of* $\tan\beta$. *Also shown in (b) is the Higgs contribution, δ_{Higgs};* **(c)** *As in (a), but as a function of $m_{\tilde{b}_1}$;* **(d)** *As a function of $m_{\tilde{t}_1}$. Remaining inputs as in Fig.4.22.*